Optimized Energy Window Configuration for ^{201}Tl Imaging

Faraz Kalantari[1], Hossein Rajabi[1], and Nahid Yaghoobi[2]

[1]Department of Medical Physics, School of Medical Sciences, Tarbiat Modares University, Tehran, Iran; and [2]Department of Nuclear Medicine, Rajaei Heart Center, Iran University of Medical Sciences, Tehran, Iran

A poor signal-to-noise ratio attributable to a low injected dose of thallium and the presence of scattered photons are the major impediments in the use of thallium as an imaging agent. Thallium decays in a complicated way and emits photons in a wide range of energies (68–82 keV). To increase the ratios of primary photons to scatter photons (primary-to-scatter ratios) and possibly increase system sensitivity, a new energy window for thallium was investigated. **Methods:** The NCAT phantom was used to simulate the distribution of activity and the attenuation coefficient in a typical patient torso. The phantom was imaged with a SPECT simulator in different energy window configurations. The energy spectra for primary photons and scatter photons were generated, and the most suitable energy windows were investigated. To evaluate the results of the simulation study, a physical phantom was imaged in different energy windows with a SPECT system. The images of the physical phantom were analyzed for the best-quality image and the corresponding window setting. To evaluate the windows determined in the simulation and phantom studies, SPECT images of 7 patients who had angiographically confirmed myocardial defects were acquired in different energy windows. The images were quantitatively compared on the basis of the calculated contrast, scatter-to-noise ratio, and sensitivity. The images were also qualitatively evaluated independently by 4 nuclear medicine specialists. **Results:** The simulation study showed that the conventional window setting (68 ± 10% keV) is not the most suitable window configuration for ^{201}Tl imaging and that the optimum energy window is 77 ± 15% keV. The images acquired in the latter window configuration yielded higher primary-to-scatter ratios, higher sensitivity (total counts), and better contrast than the images acquired in the conventional window configuration. The phantom study confirmed the results of the simulation study. In the clinical study, the images acquired in the suggested window showed a considerable increase in myocardium-to-defect contrast (1.541 ± 0.368) and myocardium-to-cavity contrast (1.171 ± 0.099) than those acquired in the conventional window configuration. **Conclusion:** The energy window configuration of 77 ± 15% keV yields higher-quality images than the conventional window configuration.

Key Words: ^{201}Tl imaging; x-ray photopeak; energy window; Monte Carlo simulation; NCAT phantom

J Nucl Med Technol 2008; 36:36–43
DOI: 10.2967/jnmt.107.043711

Thallium is a metallic element in group IIIA of the periodic table, having biologic properties similar to those of potassium (*1*). This property makes ^{201}Tl a suitable radioisotope for myocardium, parathyroid gland, and tumor imaging in nuclear medicine (*2–5*). Myocardial perfusion imaging is a widely used diagnostic procedure for the detection of cardiac artery disease and myocardial viability assessment (*6–10*).

^{201}Tl decays by electron capture to ^{201}Hg, emitting several types of γ-rays. The 2 main types of γ-rays are γ-4 of 135 keV (2.5% abundance) and γ-6 of 167 keV (9.5% abundance). The daughter element mercury has a complex spectrum of radiation; however, only x-rays of 68–82 keV (~93%) are suitable for imaging (*11*).

There are many different protocols for adjusting the energy windows in ^{201}Tl imaging (*12–18*), although commonly thallium images are acquired in 2 energy windows (*11*). The first energy window is set at the x-ray photopeak (68 ± 10% or 68 ± 15% keV), and the second window is set at the γ-6 photopeak (167 ± 20% keV). The images acquired in these 2 windows are simply summed to form images with better statistics.

This type of window setting is questionable because the x-rays emitted from ^{201}Hg are regarded as monoenergetic γ-photons of 68 keV. This presumption is not quite valid because the observed peak is not at the center of the x-ray spectrum. Therefore, substantial amounts of scatter photons are registered in the final images.

Because of the high absorbed dose and long half-time, the amount of ^{201}Tl activity administered to patients is limited, and the acquired images usually have a poor signal-to-noise ratio. In such a situation, an accurate energy window is essential to preserving the quality of the ^{201}Tl images.

The aim of the present study was to investigate the optimum energy center and width for x-rays in ^{201}Tl imaging. This investigation was performed with Monte Carlo simulated images and physical phantom images, and the results were

Received May 19, 2007; revision accepted Sep. 2, 2007.
For correspondence or reprints contact: Hossein Rajabi, PhD, Department of Medical Physics, Tarbiat Modares University, P.O. Box 14115-331, Tehran, Iran.
E-mail: hrajabi@modares.ac.ir

checked against clinical images. A comparison of the images acquired with suggested versus conventional window configurations was also performed.

MATERIALS AND METHODS

Creation of Digital Phantom

The nonuniform rational B-spline–based cardiac–torso (NCAT) digital phantom (*19,20*) was used to simulate a realistic typical patient's torso. The activity distributions in the organs of the phantom were adjusted on the basis of the ^{201}Tl uptake of the organs in a healthy person (*21*). Two small defects were fabricated on the lateral and inferoapical regions of the cardiac left ventricle. The attenuation coefficients of the tissues in the torso phantom were adjusted on the basis of the phantom attenuation coefficients of Zubal et al. (*22*). The activity and attenuation distributions of a coronal slice of the NCAT phantom are shown in Figure 1, which also shows a 3-dimensional view and a bull's-eye plot of the cardiac left ventricle.

Imaging of Digital Phantom

A SimSET (simulation system for emission tomography) Monte Carlo simulator (version 2.6.2.6; University of Washington) was used to image the virtual patient (*23*). The parameters and the dimensions of the simulator were adjusted according to Spirit DH-V (Mediso) SPECT system specifications.

The projection data were collected in a 128 × 128 matrix size with a low-energy, general-purpose (LEGP) collimator. A total of 128 views were acquired over 360° in each simulation.

Processing of Simulated images

To determine the energy spectrum of the ^{201}Tl x-rays, we performed imaging with 32 energy windows from 58 keV to 90 keV (1-keV window width, 1-keV increment). The energy spectra of the primary photons, scatter photons, and total photons were plotted (Fig. 2).

On the basis of the results shown in Figure 2, the imaging window was narrowed to 65–80 keV. To evaluate the different possible window configurations in this range of energy, we performed imaging with 16 different window configurations from 65 keV to 80 keV (1-keV increment) and 3 window widths (±10%, ±12.5%, and ±15%). The primary counts versus the center of the energy window and the ratios of primary photons to scatter photons (PTSRs) versus the center of the energy window were plotted for different window widths (Fig. 3).

To determine the most suitable energy window, we determined the window configuration in which the primary counts and the PTSRs were simultaneously maximized. To find the optimum point, we first normalized the measures of the primary counts and PTSRs to between zero and one. The corresponding normalized values of the primary counts and PTSRs were summed to provide the index of selection. The maximum value of the index was assumed to be the desired point, and the corresponding energy window configuration was determined (Fig. 4).

On the basis of the results of this simulation study, window configurations of 75 ± 15% keV and 77 ± 15% keV were determined as the potential optimum configurations.

The images acquired in these windows, those acquired in the window of 73 ± 15% keV (yielding the highest primary counts), and those acquired in the conventional on-peak window (67 ± 10% keV) were transformed to an interfile format and processed by use of the InterViewXP software package (Mediso). The images were reconstructed by use of filtered backprojection with the default processing protocols of the system. The total counts, the PTSRs, the myocardium-to-wall defect contrast, and the myocardium-to-cavity contrast were calculated as quantitative parameters for the comparisons.

Contrast was calculated as follows: contrast = (A − B)/(A + B), where A and B represent the average count in the myocardial wall

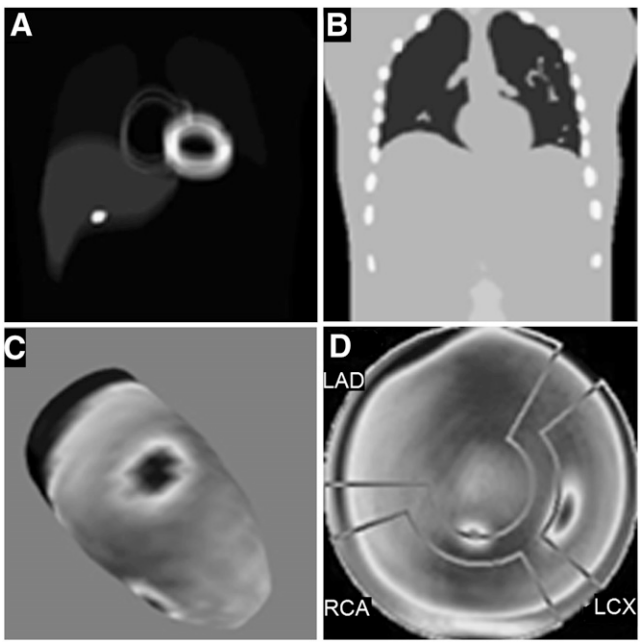

FIGURE 1. Sample images of phantom. (A) One slice of activity distribution in torso phantom. (B) Corresponding attenuation map. (C) 3-Dimensional view of cardiac left ventricle wall. (D) Bull's-eye plot of cardiac left ventricle. Images shown here are very similar to images from real patients.

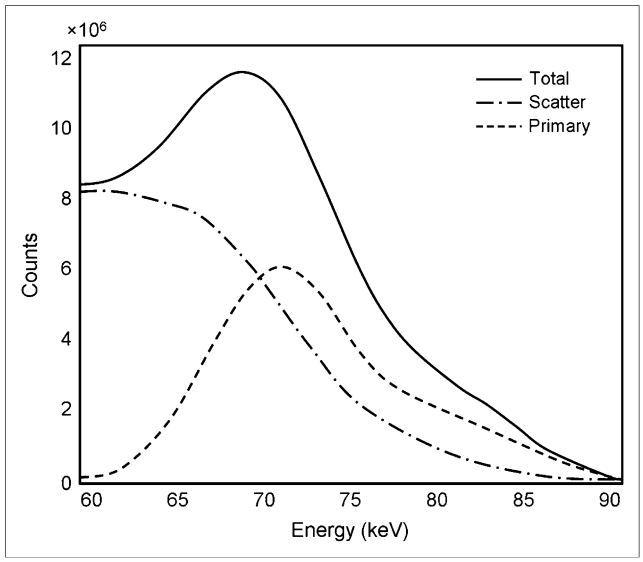

FIGURE 2. Primary, scatter, and total energy spectra of simulated ^{201}Hg x-ray photons. Graphs were generated by calculating total counts in images acquired in 32 windows from 58 keV to 90 keV at 1-keV resolution. Spectra included 167-keV photopeak counts.

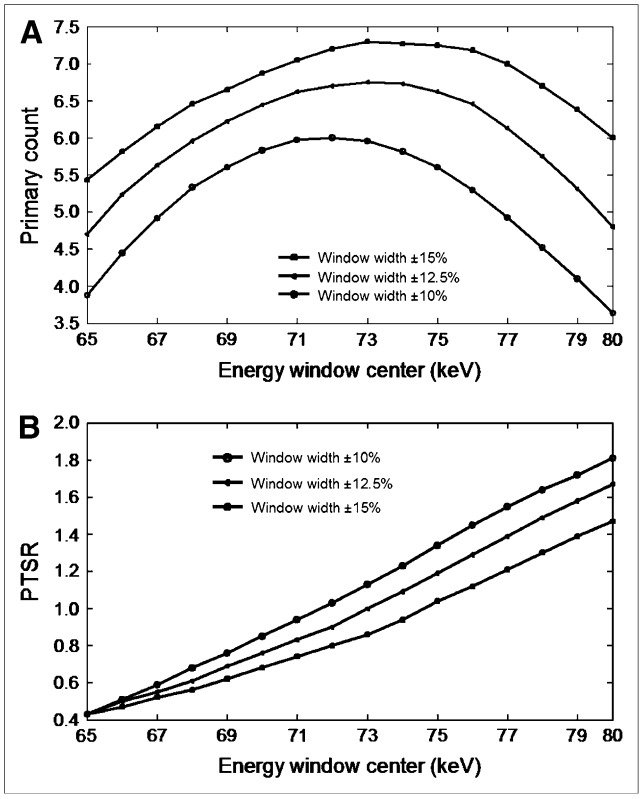

FIGURE 3. Primary counts vs. energy window centers (A) and PTSRs vs. energy window centers (B). Graphs were generated by calculating total counts in images acquired in 48 energy window configurations.

and the average count in the defect area (or ventricle cavity), respectively. The relative uptake of the myocardium was calculated by use of the bull's-eye images.

Physical Phantom Study

A Jaszczak phantom (Data Spectrum) uniformly filled with approximately 100 MBq of a ^{201}Tl aqueous solution was used as the imaging object. A dual-head SPECT system (Spirit DH-V) equipped with an LEGP collimator was used for simultaneous acquisition of the projection data in the 4 energy window configurations (all including the 167-keV photopeak). A total of 128 views in a 128 × 128 matrix size were acquired over 360° of rotation. The SPECT data were reconstructed by use of filtered backprojection as described earlier. To reduce the random fluctuation attributable to noise, data for 4 similar consecutive slices were summed.

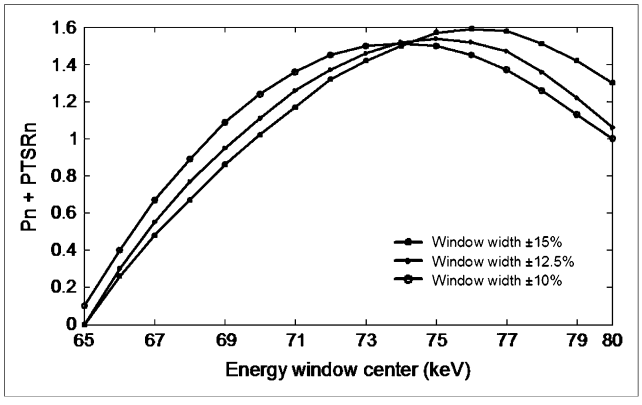

FIGURE 4. Combination of 2 graphs shown in Figure 3 after normalization. This graph simultaneously represents variations in normalized primary counts (Pn) and normalized PTSRs (PTSRn) vs. energy window centers. Maximum point in graph was assumed to represent optimum window configuration.

Identical line profiles were plotted over the images, and corresponding line profile counts were generated. The average of the peaks (maximum values) and the average of the valleys (minimum values) were determined for calculation of the image contrast.

Clinical Study

Seven patients (5 men and 2 women) who were referred for myocardial perfusion SPECT and who had a known defect, as diagnosed by angiographic data, were selected. Imaging was performed in accordance with a routine protocol; however, 3 extra images were acquired simultaneously in the energy windows of 73 ± 15% keV, 75 ± 15% keV, and 77 ± 15% keV. Projection data were collected in a 64 × 64 matrix size by use of a dual-head SPECT system (Spirit DH-V) equipped with an LEGP collimator. A total of 32 views of 60 s were acquired over 180° from left posterior oblique to right anterior oblique. The images were reconstructed as described earlier. The total counts in the projection data, the myocardium-to-defect contrast, and the myocardium-to-cavity contrast in short-axis and horizontal long-axis slices were calculated.

Four nuclear medicine physicians independently evaluated the images and selected the image that was most consistent with the results of the angiography.

RESULTS

Simulation Study

The energy spectra of the primary, the scattered, and the total photons in the range of 58–90 keV are plotted in Figure 2. Considering the relative abundance of the ^{201}Tl x-ray photons, it is clear that the photons having energies of less than 68 keV (the crossing point of the primary and the scatter spectra) were most likely to be scattered photons rather than primary photons. The majority of the photons below 68 keV originated from the higher-energy photons that lost energy because of Compton scattering in the patient's body or the collimator. This finding indicates that the conventional energy window setting (67 ± 10% keV) is not the most suitable configuration for ^{201}Tl imaging and that the center of the energy window should be set at a higher energy.

The total primary counts and the PTSRs versus the window centers (65–80 keV) for the 3 window widths (±10%, ±12.5%, and ±15%) are plotted individually in Figure 3. To determine the point at which both the primary counts and the PTSRs were optimized, we combined the corresponding curves.

To combine the curves, we normalized the measures of the primary counts and the PTSRs to 0–1 and then summed the corresponding normalized curves. The new measure was considered to be the parameter that simultaneously

involved the primary counts and the PTSRs. Variations in this new parameter versus the energy window centers are shown in Figure 4. The curve representing the window width of ±15% had a plateau peak in the range of 75–77 keV. Therefore, the center of the optimum energy window was assumed to be in this range, and the window width was assumed to be ±15%.

Another candidate considered as a potentially suitable window configuration for ^{201}Tl imaging was 73 ± 15% keV. On the basis of the results of the simulation study, this window corresponded to the maximum primary counts irrespective of the scatter photons (Fig. 3).

To determine the best of the 4 windows investigated, we compared the images acquired in these windows. The reference image in this comparison was that of the NCAT activity distribution. It was converted to planar images (similar to raw SPECT data) by use of software developed within MATLAB, version 7.0.4 (MathWorks). All of the images were transformed into an interfile format, transferred to the SPECT system, and reconstructed under the same conditions as those described earlier. The slice that included the defect and 2 adjacent slices are shown in Figure 5.

The total counts, the PTSRs, the myocardium-to-defect contrast, and the myocardium-to-cavity contrast were calculated as quantitative parameters. The myocardium-to-defect contrast was calculated by use of the counts in the ROIs drawn over the normal myocardial wall and the defect area. The average of the calculated parameters for each image is shown in Table 1.

On the basis of the results shown in Table 1, all of the investigated window configurations yielded higher PTSRs and better contrast than the conventional window configuration. Except for the window of 77 ± 15% keV, which showed a negligible reduction in sensitivity (3% fewer counts), other windows showed better sensitivity than the conventional window.

On average, the window configuration of 77 ± 15% keV yielded better results but at the cost of a negligible reduction in sensitivity. The images acquired in this window showed the most similarity to the reference images in terms of the universal image quality index (*24*).

Phantom Study

Two slices of the Jaszczak phantom acquired in different energy windows are shown in Figure 6. The total counts in the raw projection data and the average contrast calculated from the images acquired in different energy window configurations are shown in Table 2. It is clear that the images acquired in the window of 77 ± 15% keV had the highest contrast, in agreement with the results of the simulation study. The total counts (sensitivity) in this window configuration were 5% higher than those in the

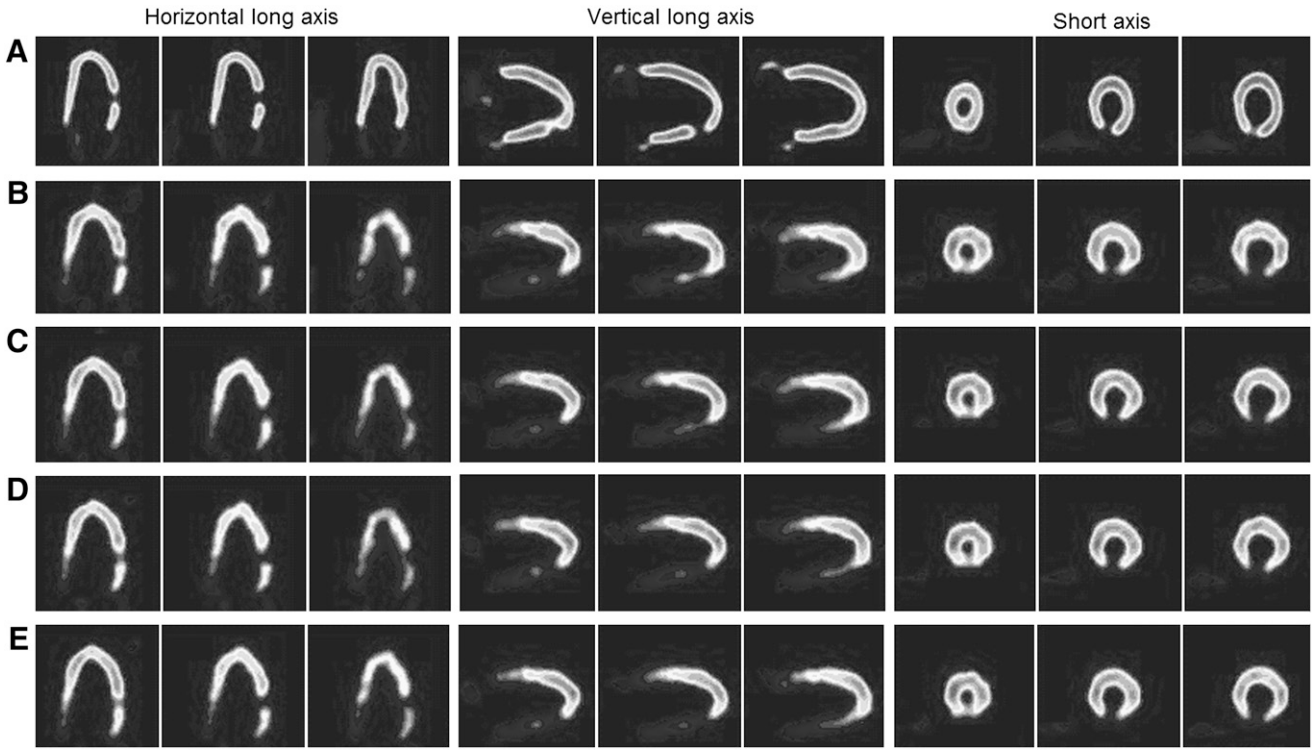

FIGURE 5. From top to bottom, 3 consecutive slices of cardiac region in NCAT phantom that was used as reference in simulation study (A), images acquired in window of 67 ± 10% keV (B), images acquired in window of 73 ± 15% keV (C), images acquired in window of 75 ± 15% keV (D), and images acquired in window of 77 ± 15% keV (E). From left to right, 3 standard views: horizontal long axis, vertical long axis, and short axis.

TABLE 1
Quantitative Parameters Derived from Simulated Images

Parameter	Value at the following window center ± width (keV):				
	68 ± 10%	73 ± 15%	75 ± 15%	77 ± 15%	Reference
Relative sensitivity	1	1.18	1.08	0.97	
PTSR	0.59	0.88	1.04	1.21	
Myocardium-to-cavity contrast	0.52	0.57	0.62	0.62	0.91
Myocardium-to-defect contrast	0.19	0.19	0.19	0.23	0.35

Images were acquired with SimSET SPECT simulator in 4 energy window configurations. Reference values were directly derived from NCAT activity distribution images. Difference between conventional window setting and window setting of 77 ± 15% keV was highly significant ($P < 0.01$), except for relative sensitivity.

conventional window configuration, whereas in the simulation study, they were 3% lower.

Four nuclear medicine physicists evaluated the images and selected the one with superior quality. Two physicists selected the images acquired in the window configuration of 77 ± 15% keV. One physicist selected the image acquired in the window configuration of 73 ± 15% keV, and the other selected the image acquired in the window configuration of 75 ± 15% keV. None of the physicists selected the image acquired in the conventional window configuration.

Clinical Study

Two adjacent slices acquired in different energy windows for one of the patients are shown in Figure 7 (3 standard views). The averages of the total counts (sensitivity) and

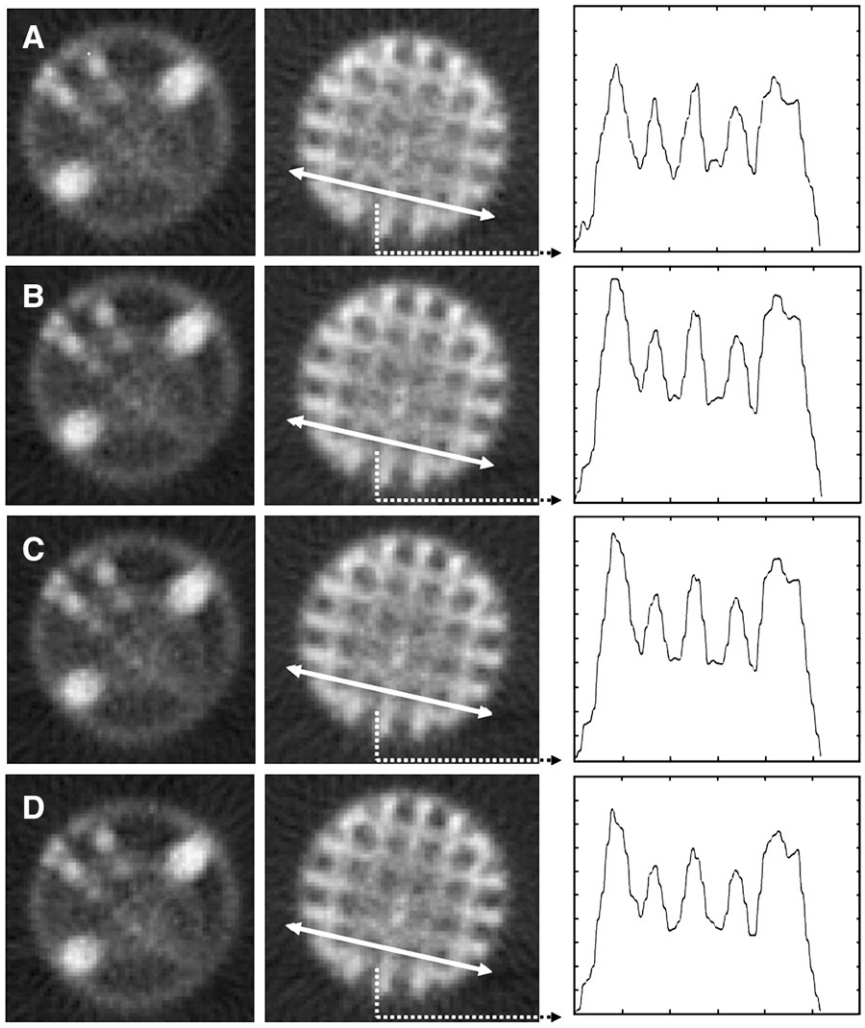

FIGURE 6. Reconstructed Jaszczak phantom images acquired in different energy window configurations: 67 ± 10% keV (A), 73 ± 15% keV (B), 75 ± 15% keV (C), and 77 ± 15% keV (D). Left image was used for visual inspection, and next was used for quantitative evaluation. Identical line profiles were used for calculation of average counts at peaks and valleys to calculate image contrast.

TABLE 2
Quantitative Parameters Derived from Jaszczak Phantom Images Acquired in Different Energy Windows

Parameter	Value at the following window center ± width (keV)			
	68 ± 10%	73 ± 15%	75 ± 15%	77 ± 15%
Relative sensitivity	1	1.28	1.14	1.05
Contrast	0.42	0.52	0.45	0.45
Physicians*	0	1	1	2

*Number of physicians who accepted corresponding images as best among 4 sets of images.

Difference between conventional window setting and window setting of 77 ± 15% keV was highly significant ($P < 0.01$), except for relative sensitivity.

the contrast calculated from the images of the patients are shown in Table 3.

Four nuclear medicine physicians evaluated the patients' images acquired in different energy window configurations and assigned a score (0–3) to each image, depending on how much it confirmed the results of angiography. The average scores are shown in Table 3.

Considering all of the factors, the conventional window configuration of 67 ± 10% keV was the worst of the windows evaluated, both quantitatively and qualitatively. However, in the energy window of 77 ± 15% keV, considerable increases in the myocardium-to-defect contrast (1.541 ± 0.368) and the myocardium-to-cavity contrast (1.171 ± 0.099) were observed. A negligible increase in the total counts in the images acquired in this window configuration was also observed. The clinical study also confirmed that the window of 77 ± 15% keV is the suitable configuration for ^{201}Tl heart imaging.

DISCUSSION

Scattered photons are among the main causes of contrast- and resolution-degrading factors in SPECT (*25*). The primary method for dealing with scattered photons is the use of a pulse-height analyzer, which rejects scattered photons on the basis of their energy (*26*). Therefore, the correct energy window setting is an important issue in nuclear medicine data acquisition (*27*). An accurate energy window setting is more important for ^{201}Tl imaging than for imaging with the other radiopharmaceuticals used in nuclear medicine. The photons emitted during ^{201}Tl disintegration are mostly x-rays having a relatively broad energy spectrum. Moreover, the administration of a low dose of ^{201}Tl results in low counting rates and poor statistics compared with those of the other radioisotopes used in nuclear medicine (*14*).

Conventionally, the center of the energy window for ^{201}Tl imaging is set over the peak of the x-ray spectrum, which is usually at about 68 keV (*5–18*). The width of the window is usually set to ±10% or ±15%. In other words, the x-rays of ^{201}Tl are implicitly considered to be monoenergetic γ-rays of 68 keV. From the physical point of view, this presumption is not quite valid because of the complex combination of primary and scattered photons in the x-ray spectrum (*28*).

The aim of the present study was to investigate the optimum energy window configuration for ^{201}Tl imaging. We tried to find the window configuration in which the PTSR would be maximized at the same time that sensitivity was preserved. This investigation was performed in 3

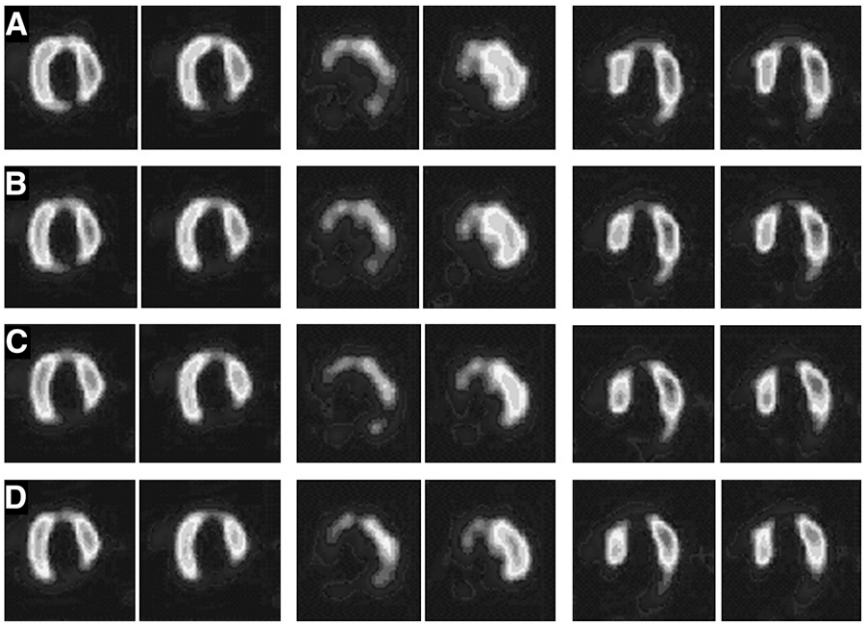

FIGURE 7. Two adjacent slices from patient images acquired in window of 67 ± 20% keV (A), window of 73 ± 15% keV (B), window of 75 ± 15% keV (C), and window of 77 ± 15% keV (D). From left to right, 3 standard views (see legend to Fig. 5).

TABLE 3
Averages of Parameters Derived from Clinical Images Acquired in Different Energy Windows

Parameter	Value at the following window center ± width (keV)			
	77 ± 15%	75 ± 15%	73 ± 15%	68 ± 10%
Relative sensitivity	1.05 ± 0.02	1.15 ± 0.02	1.24 ± 0.02	1
Relative myocardium-to-cavity contrast	1.17 ± 0.10	1.12 ± 0.09	1.07 ± 0.04	1
Relative myocardium-to-defect contrast	1.54 ± 0.37	1.33 ± 0.26	1.28 ± 0.24	1
Marks by physicians*	2.65	2.1	1.0	0.25

*Average of marks (0–3) given by physicians to images in corresponding window settings.

Except for relative sensitivity, difference between conventional window setting and window setting of 77 ± 15% keV was highly significant ($P < 0.01$).

stages: Monte Carlo simulation, Jaszczak phantom study, and clinical study. A similar investigation was previously performed (*28*); however, the phantom used in that study was a point source of activity in a cylinder filled with water as attenuation material.

Because ^{201}Tl is mainly used for heart imaging, in the present study we simulated the process by using the latest version of the SimSET Monte Carlo simulator (version 2.6.2.6) as a virtual SPECT system (*23*) and the NCAT phantom to model the torso and its organs with a realistic activity distribution and a realistic attenuation map (*19,20*). The number and distribution of the primary and scattered photons in the simulation study were similar to those in a typical clinical study (*21*). Moreover, the results of the present study were also evaluated with data from some real patients.

It was shown that the conventional symmetric energy window (68 ± 10% keV) was a less optimal choice for ^{201}Tl imaging and that the optimum energy window must be one of the following configurations: 73 ± 15% keV, 75 ± 15% keV, and 77 ± 15% keV.

In the simulation study, the downscatter of the 135- and 167-keV γ-photons into the ^{201}Tl x-ray spectrum (68–82 keV) was ignored. The lead x-ray produced in the collimator because of the collision of higher-energy γ-rays was also ignored. Because of the relatively small abundance of high-energy photons (2.5% and 9.5%), considerable error in the results of the simulation did not occur. Moreover, the large change in energy corresponded to a large deflection angle or multiple scattering and therefore even less relative abundance.

The small difference observed between relative counts recorded in the proposed and the conventional window configurations in the simulation study and the physical phantom study was partially due to ignoring the high-energy γ-rays.

In all 3 steps of this investigation, the conventional symmetric energy window (68 ± 10% keV) was found to be a less optimal choice, whereas the window of 77 ± 15% keV was proven to be the best choice.

CONCLUSION

We described a method of generating realistic simulated images with the NCAT digital torso phantom and the SimSET SPECT Monte Carlo simulator. Images were acquired in different energy window configurations. Evaluation of the acquired images showed that the conventional symmetric energy window configuration (68 ± 10% keV) was not a suitable configuration for ^{201}Tl cardiac imaging. Further analysis showed that the asymmetric window configuration of 77 ± 15% keV yielded images of superior quality compared with the conventional window configuration.

REFERENCES

1. Lebowitz E, Greene MW, Fairchild R, et al. Thallium-201 for medical use. I. *J Nucl Med.* 1975;16:151–155.
2. Sandrock D, Merino MJ, Norton JA, Neumann RD. Ultrastructural histology correlates with results of thallium-201/technetium-99m parathyroid subtraction scintigraphy. *J Nucl Med.* 1993;34:24–29.
3. Ugur O, Kostakğlu L, Güler N, et al. Comparison of ^{99m}Tc(V)-DMSA, ^{201}Tl and ^{99m}Tc-MIBI imaging in the follow-up of patients with medullary carcinoma of the thyroid. *Eur J Nucl Med.* 1996;23:1367–1371.
4. Young AE, Gaunt JI, Croft DN, Collins RE, Wells CP, Coakley AJ. Location of parathyroid adenomas by thallium-201 and technetium-99m subtraction scanning. *Br Med J (Clin Res Ed).* 1983;286:1384–1386.
5. Sugawara Y, Kikuchi T, Kajihara M, et al. Thallium-201 scintigraphy in bone and soft-tissue tumors: a comparison of dynamic, early and delayed scans. *Ann Nucl Med.* 2005;19:461–468.
6. Rozanski A, Berman DS, Gray R, et al. Use of thallium-201 redistribution scintigraphy in the preoperative differentiation of reversible and nonreversible myocardial asynergy. *Circulation.* 1981;64:936–944.
7. Matsunari I, Taki J, Nakajima K, Tonami N, Hisada K. Myocardial viability assessment using nuclear imaging. *Ann Nucl Med.* 2003;17:169–179.
8. Travin MI, Boucher CA, Newell JB, LaRaia PJ, Flores AR, Eagle KA. Variables associated with a poor prognosis in patients with an ischemic thallium-201 exercise test. *Am Heart J.* 1993;125:335–344.
9. Burkhoff D, Jones JW, Becker LC. Variability of myocardial perfusion defects assessed by thallium-201 scintigraphy in patients with coronary artery disease not amenable to angioplasty or bypass surgery. *J Am Coll Cardiol.* 2001;38:1033–1039.
10. Marin-Neto JA, Dilsizian V, Arrighi JA, et al. Thallium reinjection demonstrates viable myocardium in regions with reverse redistribution. *Circulation.* 1993;88:1736–1745.
11. Beller GA, Bergmann SR. Myocardial perfusion imaging agents: SPECT and PET. *J Nucl Cardiol.* 2004;11:71–86.
12. Hansen CL, Goldstein RA, Berman DS, et al. Myocardial perfusion and function single photon emission computed tomography. *J Nucl Cardiol.* 2006;13:e97–e120.
13. Kiat H, Germano G, Friedman J, et al. Comparative feasibility of separate or simultaneous rest thallium-201/stress technetium-99m-sestamibi dual-isotope myocardial perfusion SPECT. *J Nucl Med.* 1994;35:542–548.

14. Cao Z, Chen CC, Maunoury C, Holder LE, Abraham TC, Tehan A. Phantom evaluation of simultaneous thallium-201/technetium-99m aquisition in single-photon emission tomography. *Eur J Nucl Med.* 1996;23:1514–1520.
15. Knesaurek K, Machac J. Comparison of correction techniques for simultaneous ^{201}Tl/^{99m}Tc myocardial perfusion SPECT imaging: a dog study. *Phys Med Biol.* 2000;45:N167–N176.
16. Hademenos GJ, Dahlbom M, Hoffman EJ. Simultaneous dual-isotope technetium-99m/thallium-201 cardiac SPET imaging using a projection-dependent spilldown correction factor. *Eur J Nucl Med.* 1995;22:465–472.
17. Kadrmas DJ, Frey EC, Tsui BM. Simultaneous technetium-99m/thallium-201 SPECT imaging with model-based compensation for cross-contaminating effects. *Phys Med Biol.* 1999;44:1843–1860.
18. Moore SC, English RJ, Syravanh C, et al. Simultaneous Tc-99m/Tl-201 imaging using energy-based estimation of the spatial distributions of contaminant photons. *IEEE Trans Nucl Sci.* 1995;42:1189–1195.
19. Segars WP, Lalush DS, Tsui BMW. A realistic spline-based dynamic heart phantom. *IEEE Trans Nucl Sci.* 1999;46:503–506.
20. Segars WP, Tsui BMW. Study of the efficacy of respiratory gating in myocardial SPECT using the new 4D NCAT phantom. *IEEE Trans Nucl Sci.* 2002;49:675–679.
21. El-Ali HH, Palmer J, Carlsson M, Edenbrandt L, Ljungberg M. Comparison of 1- and 2-day protocols for myocardial SPECT: a Monte Carlo study. *Clin Physiol Funct Imaging.* 2005;25:189–195.
22. Zubal IG, Harrell CR, Smith EO, Rattner Z, Gindi G, Hoffer PB. Computerized three-dimensional segmented human anatomy. *Med Phys.* 1994;21:299–302.
23. Haynor DR, Harrison R, Lewellen TK. The use of importance sampling techniques to improve the efficiency of photon tracking in emission tomography simulations. *Med Phys.* 1991;18:990–1001.
24. Wang Z, Bovik AC. A universal image quality index. *IEEE Signal Process Lett.* 2002;9:81–84.
25. Cherry SR, Sorenson JA, Phelps ME. *Physics in Nuclear Medicine.* 3rd ed. Philadelphia, PA: Saunders; 2003.
26. Simmons GH. *The Scintillation Camera.* New York, NY: Society of Nuclear Medicine; 1988.
27. Kadrmas DJ, Frey EC, Tsui BM. Application of reconstruction-based scatter compensation to thallium-201 SPECT: implementations for reduced reconstructed image noise. *IEEE Trans Med Imaging.* 1998;17:325–333.
28. Kojima A, Takaki A, Noguchi T, et al. Optimum energy window setting on Hg-201 x-rays photopeak for effective Tl-201 imaging. *Ann Nucl Med.* 2005;19:541–547.